Same-sign WW scattering at the LHC: can we discover BSM effects before discovering new states?

Jan Kalinowski,[a,b] Paweł Kozów,[a] Stefan Pokorski,[a] Janusz Rosiek,[a] Michał Szleper[c] and Sławomir Tkaczyk [d]

[a] *Institute of Theoretical Physics, Faculty of Physics, University of Warsaw,*
ul. Pasteura 5, PL–02–093 Warsaw, Poland

[b] *CERN, Theoretical Physics Department,*
CH-1211 Geneva 23, Switzerland

[c] *National Center for Nuclear Research, High Energy Physics Department,*
ul. Hoża 69, PL-00-681, Warsaw, Poland

[d] *Fermi National Accelarator Laboratory,*
Batavia, IL 60510, USA

Abstract

It is possible that measurements of vector boson scattering (VBS) processes at the LHC will reveal disagreement with Standard Model predictions, but no new particles will be observed directly. The task is then to learn as much as possible about the new physics from a VBS analysis carried within the framework of the Effective Field Theory (EFT). In this paper we discuss issues related to the correct usage of the EFT when the WW invariant mass is not directly accessible experimentally, as in purely leptonic W decay channels. The strategies for future data analyses in case such scenario indeed occurs are proposed.

Thursday 8th February, 2018

1   Introduction and strategy

Searches for deviations from Standard Model (SM) predictions in processes involving interactions between known particles are a well established technique to study possible contributions from Beyond the Standard Model (BSM) physics. In this paper we address the question how much we can learn

about the scale of new physics and its strength using the Effective Field Theory (EFT) approach to W^+W^+ scattering if a statistically significant deviation from the SM predictions is observed in the expected LHC data for the process $pp \to 2jets + W^+W^+$. Our specific focus is on the proper use of the EFT in its range of validity. With this in mind, we discuss the practical usefulness of the EFT language to describe vector boson scattering (VBS) data and whether or not this can indeed be the right framework to observe the first hints of new physics at the LHC.

The EFT is in principle a model independent tool to describe BSM physics below the thresholds for new states. One supplements the SM Lagrangian by higher dimension operators

$$\mathcal{L} = \mathcal{L}_{SM} + \Sigma_i \frac{C_i^{(6)}}{\Lambda_i^2} \mathcal{O}_i^{(6)} + \Sigma_i \frac{C_i^{(8)}}{\Lambda_i^4} \mathcal{O}_i^{(8)} + ... \tag{1.1}$$

where the C's are some "coupling constants" and Λ's are the decoupled new mass scales. The mass scale is a feature of the UV completion of the full theory and thus is assumed common to all the coefficients

$$f_i^{(6)} = \frac{C_i^{(6)}}{\Lambda^2}, \qquad f_i^{(8)} = \frac{C_i^{(8)}}{\Lambda^4}, ... \tag{1.2}$$

which are free parameters because the full theory is unknown. One should stress that the usefulness of any EFT analysis of a given process relies on the assumption that only few terms in the expansion of Eq. (1.1) give for that process an adequate approximation to the underlying UV theory. The necessary condition obviously is that the energy scale of the considered process, $E < \Lambda$. However, the effective parameters in the expansion Eq. (1.1) are the f's and not the scale Λ itself. Neither Λ nor the C's are known without referring to specific UV complete models. Even for $E << \Lambda$ a simple counting of powers of E/Λ can be misleading as far as the contribution of various operators to a given process is concerned. The latter depends also on the relative magnitude of the couplings C, e.g., $C_i^{(6)}$ versus $C_i^{(8)}$ and/or within each of those sets of operators, separately, [1–4], as well as on the interference patterns in various amplitudes calculated from the Lagrangian Eq. (1.1) [5].

For instance, the contribution of dimension-6 (D=6) operators to a given process can be suppressed compared to dimension-8 (D=8) operators contrary to a naive (E/Λ) power counting [3–6] or, vice versa, the [SM × D=8] interference contribution can be subleading with respect to the $[D = 6]^2$ one [2, 4, 7]. Clearly, the assumption about the choice of operators in the truncation in Eq. (1.1) used to analyze a process of our interest introduces a strong model dependent aspect of that analysis: one is implicitly assuming that there exist a class of UV complete models such that the chosen truncation is a good approximation. It is convenient to introduce the concept of EFT "models" defined by the choice of operators $\mathcal{O}_i$ and the values of f_i. The question of this paper is then about the discovery potential at the LHC for BSM physics described by various EFT "models".

The crucial question is what the range of validity can be of a given EFT "model". There is no precise answer to this question unless one starts with a specific theory and derives Eq. (1.1) by decoupling the new degrees of freedom. However, in addition to the obvious constraint that the EFT approach can be valid only for the energy scale $E < \Lambda$ (unfortunately with unknown value of Λ), for theoretical consistency the partial wave amplitudes should satisfy the perturbative unitarity condition. The latter requirement translates into the condition $E^2 < \Lambda^2 \le s^U$, where $s^U \equiv s^U(f_i)$ is the perturbative partial wave unitarity bound as a function of the chosen operators and the values of the coefficients f_i's. Thus, the value of $\Lambda_{max}^2 = s^U$ gives the upper bound on the validity of the EFT based "model". Since the magnitude of the expected (or observed) experimental effects also depends

on the same f_i, one has a frame for a consistent use of the EFT "model" to describe the data once they are available. For a BSM discovery in the EFT framework, proper usage of the "model" is a vital issue. It makes no physical sense to extend the EFT "model" beyond its range of applicability, set by the condition $E < \Lambda$. We shall illustrate this logic in more detail in the following.

A common practice in the LHC data analyses in the EFT framework is to derive uncorrelated limits on one dimension-8 operator at a time while setting all the remaining Wilson coefficients to zero. Strictly speaking, such limits are valid only under the assumption that just one such operator dominates BSM effects in the studied process in the available energy range. For simplicity, in this paper we also consider single dimension-8 operators at a time, keeping in mind that varying more than one operator substantially complicates the analysis. For a given EFT "model"

$$\sigma \propto |A_{full}|^2 = |A_{SM}|^2 + (A_{SM} \times A_{BSM}^* + hc) + |A_{BSM}|^2. \tag{1.3}$$

We focus on the process

$$pp \rightarrow 2jets + W^+W^+ \rightarrow 2jets + l^+\nu + l'^+\nu' \tag{1.4}$$

where l and l' stand for any combination of electrons and muons. The process depends on the W^+W^+ scattering amplitude (the gauge bosons can of course be virtual). The EFT "models" can be maximally valid up to certain invariant mass $M = \sqrt{s}$ of the W^+W^+ system

$$M < \Lambda \leq M^U(f_i) \tag{1.5}$$

where $M^U(f_i)$ is fixed by the partial wave perturbative unitarity constraint, $(M^U(f_i))^2 = s^U(f_i)$.

The differential cross section $\frac{d\sigma}{dM}$ reads (actual calculations must include also all non-VBS diagrams leading to the same final states):

$$\frac{d\sigma}{dM} \sim \Sigma_{ijkl} \int dx_1 dx_2 q_i(x_1) q_j(x_2) |\mathcal{M}(ij \rightarrow klW^+W^+)|^2 d\Omega\, \delta(M - \sqrt{(p_{W^+} + p_{W^+})^2}) \tag{1.6}$$

where $q_i(x)$ is the PDF for parton i, the sum runs over partons in the initial (ij) and final (kl) states and over helicities, the amplitude $\mathcal{M}$ is for the parton level process $ij \rightarrow klW^+W^+$ and $d\Omega$ denotes the final state phase space integration. The special role of the distribution $\frac{d\sigma}{dM}$ follows from the fact that it is straightforward to impose the cutoff $M \leq \Lambda$, Eq. (1.5), for the WW scattering amplitude. The differential cross section, $\frac{d\sigma}{dM}$, is therefore a very sensitive and straightforward test of new physics defined by a given EFT "model". Unfortunately, the W^+W^+ invariant mass in the purely leptonic W decay channel is not directly accessible experimentally and one has to investigate various experimental distributions of the charged particles. The problem here is that the kinematic range of those distributions is not related to the EFT "model" validity cutoff $M < \Lambda$ and if $\Lambda < M_{max}$, where M_{max} is the kinematic limit accessible at the LHC for the WW system, there is necessarily also a contribution to those distributions from the region $\Lambda < M < M_{max}$. The question is then: in case a deviation from SM predictions is indeed observed, how to verify a "model" defined by a single higher-dimension operator $\mathcal{O}_i^{(k)}$ and a given value of f_i by fitting it to a set of experimental distributions D_i and in what range of f_i such a fit is really meaningful [7]. Before we address this question, it is in order to comment on the perturbative partial wave unitarity constraint.

It is worthwhile to stress several interesting points.

1. For a given EFT "model", the unitarity bound is very different for the $J = 0$ partial wave of different helicity amplitudes and depends on their individual energy dependence (some of them remain even constant and never violate unitarity, see Appendix). Our M^U has to be taken as the *lowest* unitarity bound, universally for all helicity amplitudes, because it is the lowest bound that determines the scale Λ_{max}. More precisely, one should take the value obtained from diagonalization of the matrix of the $J = 0$ partial waves in the helicity space.

2. Correct assessment of the EFT "model" validity range in the W^+W^+ scattering process requires also consideration of the W^+W^- scattering amplitudes which by construction probe the same couplings and are sensitive to exactly the same operators. For most higher dimension operators, this actually significantly reduces their range of validity in W^+W^+ analyses. Conversely, the WZ and ZZ processes can be assumed to contain uknown contributions from additional operators which adjust the value of Λ consistently.

3. It is interesting to note that below the value of M^U the deviations from SM predictions in the total cross sections are sizable only in a narrow range of energies. They are mainly due to the interference term in Eq. (1.3). Even if deviations from the SM are dominated by the helicity combinations that reach the unitarity bound first, the total unpolarized cross sections up to $M = M^U$ get important contributions also from amplitudes which are still far from their own unitarity limits.

In the Appendix we illustrate various aspects of those bounds by presenting the results of analytical calculations for two dimension-8 operators, one contributing mainly to the scattering of longitudinally polarized gauge bosons and one to transversely polarized.

We now come back to the problem of testing the EFT "models" when the W^+W^+ invariant mass is not accesible experimentally. Let us define the BSM signal as the deviation from the SM prediction in the distribution of some observable D_i.

$$S = D_i^{model} - D_i^{SM}. \tag{1.7}$$

The first quantitative estimate of the signal can be written as

$$D_i^{model} = \int_{2M_W}^{\Lambda} \frac{d\sigma}{dM}|_{model} dM + \int_{\Lambda}^{M_{max}} \frac{d\sigma}{dM}|_{SM} dM. \tag{1.8}$$

It is the most conservative estimate since it assumes only the SM contribution in the region $M > \Lambda$. Realistically one expects some BSM contribution also from the region above Λ. While this additional contribution may enhance the signal and thus our sensitivity to new physics, it may also preclude proper description of the data in the EFT language. Such description in terms of a particular EFT "model" makes sense if and only if this contribution is small enough when compared to the contribution from the region controlled by the EFT "model". The latter depends on the value of Λ and f_i, and the former on the unknown physics for $M > \Lambda$, which regularizes the scattering amplitudes and makes them consistent with partial wave unitarity. Ideally, one would conclude that the EFT "model" is tested for values of $(\Lambda \leq M^U, f_i)$ such that the signals computed from Eq. (1.8) are statistically consistent (say, within 2 standard deviations) with the signals computed when the tail $\Lambda > M^U$ is modeled in **any** way that preserves unitarity of the amplitudes. That

4

requirement is, of course, impossible to impose but, fortunately, for large enough values of Λ, this region is driven by the tails of the parton distributions and its contribution can be expected to be indeed suppressed, and only weakly dependent on the details of the amplitudes above Λ. For a rough quantitative estimate of the magnitude of this contribution, one can assume that all the helicity amplitudes above Λ remain constant at their respective values they reach at Λ, and that Λ is common to all the helicity amplitudes. For $\Lambda = \Lambda_{max}$, this prescription regularizes the helicity amplitudes that violate unitarity at M^U and also properly accounts for the contributions of the helicity amplitudes that remain constant with energy. It gives a reasonable approximation to the total unpolarized cross sections for $M > M^U$, at least after some averaging over M. More elaborated regularization techniques can also be checked here. The full contribution to a given distribution D_i is then taken as

$$D_i^{model} = \int_{2M_W}^{\Lambda} \frac{d\sigma}{dM}|_{model} dM + \int_{\Lambda}^{M_{max}} \frac{d\sigma}{dM}|_{A=const} dM \qquad (1.9)$$

BSM observability imposes some minimum value of f to obtain the required signal statistical significance. It can be derived based on Eq. (1.9) (or Eq. (1.8)). On the other hand, description in the EFT language imposes some maximum value of f such that signal estimates computed from Eqs. (1.8) and (1.9) remain statistically consistent. Large difference between the two computations implies significant sensitivity to the region above Λ. It impedes a meaningful data description in the EFT language and also suggests we are more likely to observe the new physics directly.

Assuming $\Lambda = M^U$, we get a finite interval of possible f values, bounded from two sides, for which BSM discovery and correct EFT description are both plausible. In the more general case when $\Lambda < M^U$, i.e., new physics states may appear before our EFT "model" reaches its unitarity limit, respective limits on f depend on the actual value of Λ. We thus obtain a 2-dimensional region in the plane (Λ, f_i), which is shown in the cartoon plot in Fig. 1. This region is bounded from above by the unitarity bound $M^U(f_i)$ (solid blue curve), from the left by the signal significance criterion (dashed black curve) and from the right by the EFT consistency criterion (dotted black curve). The EFT could be the right framework to search for BSM physics as long as these three criteria do not mutually exclude each other, i.e., graphically, the "triangle" shown in our cartoon plot is not empty. In Section 3 we will verify whether such "triangles" indeed exist for the individual dimension-8 operators.

Thus, our preferred strategy for data analysis is as follows:

1. From collected data measure a distribution D_i (possibly in more than one dimension) that is found from simulation work to offer the highest sensitivity to new physics effects,

2. If deviations from the SM are indeed observed [1], fit particular values of $(\Lambda \leq M^U, f_i)$ based on EFT simulated samples in which the contribution from the region $M > \Lambda$ is taken into account according to Eq. (1.9) or using some more elaborated regularization methods,

3. Fixing f_i and Λ to the fit values, recalculate the distribution D_i such that the region $M > \Lambda$ is populated only by the SM contribution (Eq. (1.8)),

---

[1] We do not discuss in this paper the bounds on the Wilson coefficients obtained from the data analysis when no statistically significant signal on new physics is observed. Such an analysis requires a separate discussion, although it will be also influenced by the results of this paper.
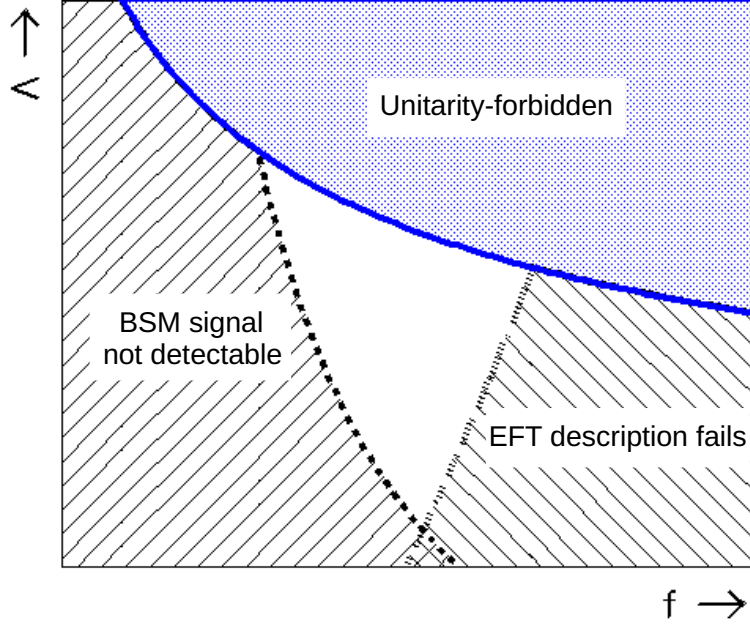
Figure 1: Cartoon plot which shows the regions in f_i and Λ (for an arbitrary higher-dimension operator $\mathcal{O}_i$) in terms of BSM signal observability and applicability of EFT "models" based on the choice of a higher-dimension operator in an analysis of the same-sign VBS process with purely leptonic decays. The central white triangle is the most interesting region where the underlying BSM physics can be studied within the EFT framework.

4. Check statistical consistency between the original simulated D_i and the one based on Eq. (1.8),

5. Physics conclusions from the obtained (Λ, f_i) values can only be drawn if such consistency is found.

2 Preliminary technicalities

The same-sign $pp \to W^+W^+jj$ process probes a number of higher dimension operators. Among them are dimension-6 operators which modify only the Higgs-to-gauge coupling:

$$\begin{aligned}
\mathcal{O}_{\Phi d} &= \partial_\mu(\Phi^\dagger\Phi)\partial^\mu(\Phi^\dagger\Phi), \\
\mathcal{O}_{\Phi W} &= (\Phi^\dagger\Phi)\mathrm{Tr}[W^{\mu\nu}W_{\mu\nu}], \\
\mathcal{O}_{\tilde{W}W} &= \Phi^\dagger\tilde{W}_{\mu\nu}W^{\mu\nu}\Phi
\end{aligned} \tag{2.1}$$

(the last one being CP-violating), dimension-6 operators which induce anomalous triple gauge couplings (aTGC):

$$\begin{aligned}
\mathcal{O}_{WWW} &= \mathrm{Tr}[W_{\mu\nu}W^{\nu\rho}W_\rho^\mu], \\
\mathcal{O}_W &= (D_\mu\Phi)^\dagger W^{\mu\nu}(D_\nu\Phi), \\
\mathcal{O}_B &= (D_\mu\Phi)^\dagger B^{\mu\nu}(D_\nu\Phi), \\
\mathcal{O}_{\tilde{W}WW} &= \mathrm{Tr}[\tilde{W}_{\mu\nu}W^{\nu\rho}W_\rho^\mu], \\
\mathcal{O}_{\tilde{W}} &= (D_\mu\Phi)^\dagger\tilde{W}^{\mu\nu}(D_\nu\Phi)
\end{aligned} \tag{2.2}$$

6

(the last two of which are CP-violating), as well as dimension-8 operators which induce only anomalous quartic couplings (aQGC). In the above, Φ is the Higgs doublet field, the covariant derivative is defined as

$$D_\mu \equiv \partial_\mu + i\frac{g'}{2}B_\mu + igW_\mu^i\frac{\tau^i}{2} \tag{2.3}$$

and the field strength tensors are

$$W_{\mu\nu} = \frac{i}{2}g\tau^i(\partial_\mu W_\nu^i - \partial_\nu W_\mu^i + g\epsilon_{ijk}W_\mu^j W_\nu^k),$$
$$B_{\mu\nu} = \frac{i}{2}g'(\partial_\mu B_\nu - \partial_\nu B_\mu) \tag{2.4}$$

for gauge fields W_μ^i and B_μ of $SU(2)_I$ and $U(1)_Y$, respectively.

Higgs and triple gauge couplings can be accessed experimentally via other processes, namely Higgs physics and diboson production which is most sensitive to aTGC. They are presently known to agree with the SM within a few per cent [13], which translates into stringent limits on the dimension-6 operators.

On the other hand, VBS processes are more suitable to constrain aQGC. The following dimension-8 operators contribute to the $WWWW$ vertex:

$$\mathcal{O}_{S0} = \left[(D_\mu\Phi)^\dagger D_\nu\Phi\right] \times \left[(D^\mu\Phi)^\dagger D^\nu\Phi\right],$$
$$\mathcal{O}_{S1} = \left[(D_\mu\Phi)^\dagger D^\mu\Phi\right] \times \left[(D_\nu\Phi)^\dagger D^\nu\Phi\right],$$
$$\mathcal{O}_{M0} = \mathrm{Tr}\left[\hat{W}_{\mu\nu}\hat{W}^{\mu\nu}\right] \times \left[(D_\beta\Phi)^\dagger D^\beta\Phi\right],$$
$$\mathcal{O}_{M1} = \mathrm{Tr}\left[\hat{W}_{\mu\nu}\hat{W}^{\nu\beta}\right] \times \left[(D_\beta\Phi)^\dagger D^\mu\Phi\right],$$
$$\mathcal{O}_{M6} = \left[(D_\mu\Phi)^\dagger \hat{W}_{\beta\nu}W^{\beta\nu}D^\mu\Phi\right], \tag{2.5}$$
$$\mathcal{O}_{M7} = \left[(D_\mu\Phi)^\dagger \hat{W}_{\beta\nu}\hat{W}^{\beta\mu}D^\nu\Phi\right],$$
$$\mathcal{O}_{T0} = \mathrm{Tr}\left[\hat{W}_{\mu\nu}\hat{W}^{\mu\nu}\right] \times \mathrm{Tr}\left[\hat{W}_{\alpha\beta}\hat{W}^{\alpha\beta}\right],$$
$$\mathcal{O}_{T1} = \mathrm{Tr}\left[\hat{W}_{\alpha\nu}\hat{W}^{\mu\beta}\right] \times \mathrm{Tr}\left[\hat{W}_{\mu\beta}\hat{W}^{\alpha\nu}\right],$$
$$\mathcal{O}_{T2} = \mathrm{Tr}\left[\hat{W}_{\alpha\mu}\hat{W}^{\mu\beta}\right] \times \mathrm{Tr}\left[\hat{W}_{\beta\nu}\hat{W}^{\nu\alpha}\right].$$

In the above, we have defined $\hat{W}_{\mu\nu} = \frac{1}{ig}W_{\mu\nu}$. Throughout this paper we follow the convention used in MadGraph [16] with dimension-8 operators included via public UFO files as far as the actual definitions of the field strength tensors and Wilson coefficients are concerned. Whenever results from the VBFNLO program [17] are used in this work, appropriate conversion factors are applied. For more details on the subject see Ref. [11].

The same-sign $pp \to W^+W^+jj$ production has been already observed during Run I of the LHC [8,9] and confirmed by a recent measurement of the CMS Collaboration at 13 TeV Run II [10]. Also, pioneering measurements of the $ZW^\pm jj$ [14] and $ZZjj$ [15] processes exist. They all place experimental limits on the relevant dimension-8 operators. However, most presently obtained limits involve unitarity violation within the measured kinematic range, leading to problems in physical interpretation and even comparison of the different analyses.

Our goal is to investigate the discovery potential at the High Luminosity LHC (HL-LHC) of the BSM physics effectively described by EFT "models" with single dimension-8 operators at a time, with proper attention paid to the regions of validity of such models, as described in Section 1.

3 Results of simulations

For the following analysis dedicated event samples of the process $pp \to jj\mu^+\mu^+\nu\nu$ at 14 TeV were generated at LO using the MadGraph5_aMC@NLO v5.2.2.3 generator [16], with the appropriate UFO files containing additional vertices involving the desired dimension-8 operators. For each dimension-8 operator a sample of at least 500,000 events within a phase space consistent with a VBS-like topology (defined below) was generated. A preselected arbitrary value of the relevant f coefficient (from now on, $f \equiv f_i$ with $i = S0, S1, T0, T1, T2, M0, M1, M6, M7$) was assumed at each generation; different f values were obtained by applying weights to generated events, using the reweight command in MadGraph. The value $f=0$ represents the Standard Model predictions for each study. The Pythia package v6.4.1.9 [18] was used for hadronization as well as initial and final state radiation processes. No detector was simulated. Cross sections at the output of MadGraph were multiplied by a factor 4 to account for all the lepton (electron and/or muon) combinations in the final state.

In this analysis, the Standard Model process $pp \to jjl^+l^+\nu\nu$ is treated as the irreducible background, while signal is defined as the enhancement (which may be positive or negative in particular cases) of the event yield in the presence of a given dimension-8 operator relative to the Standard Model prediction. No reducible backgrounds were simulated, as they are known to be strongly detector dependent. For this reason, results presented here should be treated mainly as a demonstration of our strategy rather than as a precise determination of numerical values. For more realistic results this analysis should be repeated with full detector simulation for each of the LHC experiments separately.

The final analysis is performed by applying standard VBS-like event selection criteria, similar to those applied in data analyses carried by ATLAS and CMS. These were: $M_{jj} > 500$ GeV, $\Delta\eta_{jj} > 2.5$, $p_T^j > 30$ GeV, $|\eta_j| < 5$, $p_T^l > 25$ GeV, $|\eta_l| < 2.5$. For each f value of every dimension-8 operator, signal significance is assessed by studying the distribiutions of a large number of kinematic variables. Signal significance expressed in standard deviations (σ) is defined as the square root of a χ^2 resulting from comparing the bin-by-bin event yields, normalized to a total integrated luminosity of 3 ab^{-1}, in a given dimension-8 scenario and in the Standard Model. We only considered one-dimensional distributions of single variables. Each distribution was divided into 10 bins, arranged so that the Standard Model prediction in each bin is never lower than 2 events. Overflows were always included in the respective highest bins. Examples of such distributions are shown in Fig. 2. For each dimension-8 operator we took the distribution that produced the highest χ^2 among the considered variables. The most sensitive variables we found to be $R_{p_T} \equiv p_T^{l1} p_T^{l2}/(p_T^{j1} p_T^{j2})$ [19] for $\mathcal{O}_{S0}$ and $\mathcal{O}_{S1}$, and $M_{o1} \equiv \sqrt{(|\vec{p}_T^{\,l1}| + |\vec{p}_T^{\,l2}| + |\vec{p}_T^{\,miss}|)^2 - (\vec{p}_T^{\,l1} + \vec{p}_T^{\,l2} + \vec{p}_T^{\,miss})^2}$ [20] for the remaining operators (for some of them, M_{ll} would give almost identical results as M_{o1}, but usually this was not the case).

As anticipated in Section 1, signal is calculated in two ways. First, using Eq. (1.8), where Λ can vary in principle between $2M_W$ and the appropriate unitarity limit for each chosen value of f_i.

The $M_{WW} > \Lambda$ tail of the distribution is then assumed identical as in the Standard Model case. Second, using Eq. (1.9) which accounts for an additional BSM contribution coming from the region $M_{WW} > \Lambda$. The latter is estimated under the assumption that helicity amplitudes remain constant above this limit, as discussed in Section 1. For the case when Λ is equal to the unitarity limit, this corresponds to unitarity saturation. An additional χ^2 is computed based on the comparison of the respective kinematic distributions in the two considered signal scenarios for each given f. This number quantifies our experimental sensitivity to the unknown region $M_{WW} > \Lambda$.

Unitarity limits were computed using the VBFNLO [17] calculator v1.3.0, after applying appropriate conversion factors to the input values of the Wilson coeeficients, so to make it suitable to the MadGraph 5 convention. We used the respective values from T-matrix diagonalization, considering both W^+W^+ and W^+W^- channels, and taking always the lower value of the two. For the operators we consider here, unitarity limits are lower for W^+W^- than for W^+W^+ except for f_{S0} (both positive and negative) and negative f_{T1}.

In this analysis, Eq. (1.9) was implemented by applying additional weights to events above $M_{WW} = \Lambda$ in the original non-regularized samples generated by MadGraph. For the dimension-8 operators, this weight was equal to $(\Lambda/M_{WW})^4$. The choice of the power in the exponent takes into account that the non-regularized total cross section for WW scattering grows less steeply around $M_{WW} = \Lambda$ than its asymptotic behavior $\sim s^3$, which is valid in the limit $M_{WW} \to \infty$. This follows from the observation that unitarity is first violated much before the cross section gets dominated by its $\sim s^3$ term, as shown in the Appendix. The applied procedure is supposed to ensure that the total WW scattering cross section after regularization behaves like $1/s$ for $M_{WW} > \Lambda$, and so it approximates the principle of constant amplitude (Section 1), at least after some averaging over the individual helicity combinations.

Lower observation limits on each operator are defined by the requirement of signal significance being above the 5σ level. Small differences between the respective signal predictions obtained using Eqs. (1.8) and (1.9), as well as using other regularization techniques, will be manifest as slightly different observation limits and should be understood as the uncertainty margin arising from the unknown physics above Λ, no longer described in terms of the EFT. Examples of signal significances as a function of f are shown in Fig. 3 with dashed curves. Consistency of the EFT description is determined by requiring a small χ^2 between the respective predictions from Eqs. (1.8) and (1.9). In this analysis we allowed differences amounting to up to 2σ in the most sensitive kinematic distribution. This difference as a function of f is shown in Fig. 3 as dotted curves. These considerations consequently translate into effective upper limits on the value of f for each operator.

Assuming Λ is equal to the respective unitarity bounds, the lower and upper limits for the values of f for each dimension-8 operator, for positive and negative f values, estimated for the HL-LHC with an integrated luminosity of 3 ab^{-1}, are read out directly from graphs such as Fig. 3 and listed below in Table 1. These limits define the (continous) sets of testable EFT "models" based on the choice of single dimension-8 operators.

The fact that the obtained lower limits are more optimistic than those from several earlier studies (see, e.g., Ref. [21]) reflects our lack of detector simulation and reducible background treatment, but may be partly due to the use of the most sensitive kinematic variables. It must be stressed, nonetheless, that both these factors affect all lower and upper limits likewise, so their relative positions with respect to each other are unlikely to change much.

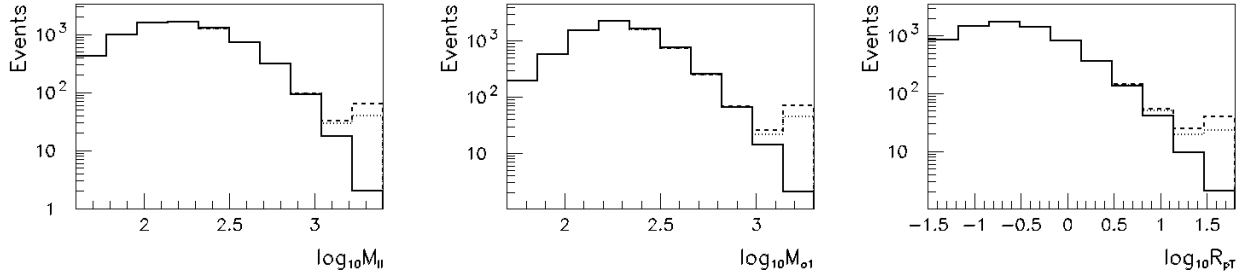As can be seen, the ranges are rather narrow, but in most cases non-empty. Rather wide regions

Figure 2: Typical examples of kinematic distributions used for the assessment of BSM signal significances. Shown are the distributions of M_{ll}, M_{o1} and R_{pT} (in log scale): in the Standard Model (solid lines), with f_{T1}=0.1/TeV^{-4} and the high-M_{WW} tail treatment according to Eq. (1.9) (dashed lines), and with f_{T1}=0.1/TeV^{-4} and the high-M_{WW} tail treatment according to Eq. (1.8) (dotted lines). Assumed is $\sqrt{s} = 14$ TeV and an integrated luminosity of 3 ab^{-1}.
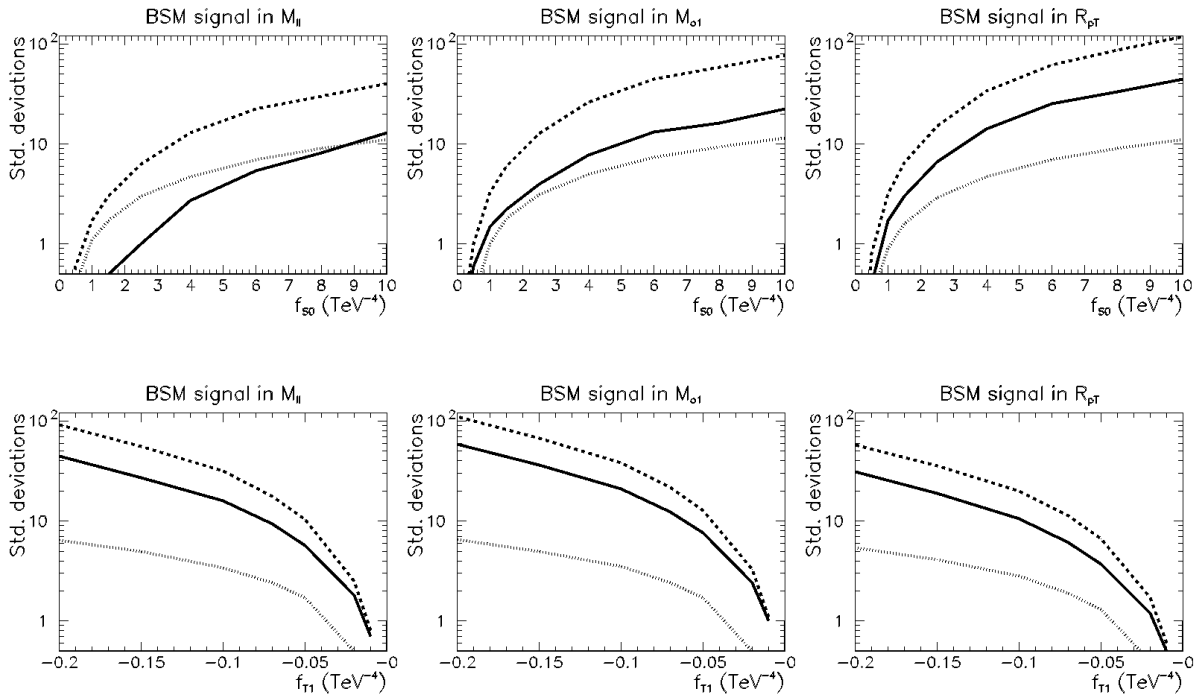

Figure 3: Typical examples of BSM signal significances computed as a function of f_{S0} (upper row) and f_{T1} (lower row) based on different kinematic distributions. Here the Λ cutoff is assumed equal to the unitarity limit. Shown are predictions obtained by using Eq. (1.8) (solid lines) and Eq. (1.9) (dashed lines). The dotted lines show the difference in standard deviations between the two respective calculations. Assumed is $\sqrt{s} = 14$ TeV and an integrated luminosity of 3 ab^{-1}.

10

Coeff.	Lower limit (TeV^{-4})	Upper limit (TeV^{-4})	Coeff.	Lower limit (TeV^{-4})	Upper limit (TeV^{-4})
f_{S0}	1.3	2.0	$-f_{S0}$	1.2	2.0
f_{S1}	8.0	6.5	$-f_{S1}$	5.5	6.0
f_{T0}	0.08	0.13	$-f_{T0}$	0.05	0.12
f_{T1}	0.03	0.06	$-f_{T1}$	0.03	0.06
f_{T2}	0.20	0.25	$-f_{T2}$	0.10	0.20
f_{M0}	1.0	1.2	$-f_{M0}$	1.0	1.2
f_{M1}	1.0	1.9	$-f_{M1}$	0.9	1.8
f_{M6}	2.0	2.4	$-f_{M6}$	2.0	2.4
f_{M7}	1.1	2.8	$-f_{M7}$	1.3	2.8

Table 1: Estimated lower limits for BSM signal significance and upper limits for EFT consistency for each dimension-8 operator (positive and negative f values), for the case when Λ is equal to the unitarity bound, in the W^+W^+ scattering process at the LHC with 3 ab^{-1}.

where BSM signal significance does not preclude consistent EFT description can be identified for f_{T1} and f_{M7} regardless of sign, as well as somewhat smaller regions for f_{T0}, f_{T2} and f_{M1}. Prospects for f_{M0}, f_{M6} and f_{S0} may depend on the accuracy of the high-M_{WW} tail modeling and a narrow window is also likely to open up unless measured signal turns out very close to its most conservative prediction. Only for positive values of f_{S1}, the resulting upper limit for consistent EFT description remains entirely below the lower limit for signal significance.

Allowing that the scale of new physics Λ may be lower than the actual unitarity bound results in 2-dimensional limits in the (f, Λ) plane. Usually this means further reduction of the allowed f ranges for lower Λ values and the resulting regions take the form of an irregular triangle. Respective results for all the dimension-8 operators are depicted in Figs. 4 and 5. It is interesting to note that in many cases this puts an effective lower limit on Λ itself, in addition to the upper limit derived from the unitarity condition. In particular, the adopted criteria bound the value of Λ to being above $\sim$2 TeV for the $\mathcal{O}_M$ operators as well as for $\mathcal{O}_{S0}$. The $\mathcal{O}_T$ operators still allow a wider range of Λ. Unfortunately, there is little we can learn from fitting f_{S1}, since signal observability requires very low Λ values, for which the new physics could probably be detected directly.

It is interesting to plot the values of the couplings $\sqrt{C}$ in Eq. (1.1) as a function of f_i assuming $\Lambda_{max} = M^U$ i.e., $C_{max} = f \times (M^U)^{k-4}$, where k is the dimensionality of the operator that defines the EFT "model". In models with one BSM scale and one BSM coupling constant $\sqrt{C}$ has the interpretation of the coupling constant [1]. The values of C_{max} are to a good approximation independent of f (see Fig. 6) and, being generally in the range $(\sqrt{4\pi}, 4\pi)$, reflect the approach to a strongly interacting regime in an underlying (unknown) UV complete theory. The EFT discovery regions depicted in Figs. 4 and 5 have further interesting implications for the couplings C. For a fixed f, the unitarity bound $\Lambda^2 < s^U$ implies that $C < C_{max} = f(M^U)^4$, whereas the lower bound on Λ that comes from the combination of the signal significance and EFT consistency criteria gives us $C > \Lambda_{min}^4 f$. Thus, a given range $(\Lambda_{min}, \Lambda_{max})$ corresponds to a range of values of the couplings C, so that we could not only discover an indirect sign of BSM physics, but also learn something

about the nature of the complete theory, whether it is strongly or weakly interacting. In particular, for the following operators: $\mathcal{O}_{S0}$, $\mathcal{O}_{M0}$, $\mathcal{O}_{M1}$, $\mathcal{O}_{M6}$ and $\mathcal{O}_{M7}$, only models with C being close to the strong interaction limit will be experimentally testable, while a wider range of C may be testable for $\mathcal{O}_{T0}$, $\mathcal{O}_{T1}$ and $\mathcal{O}_{T2}$.
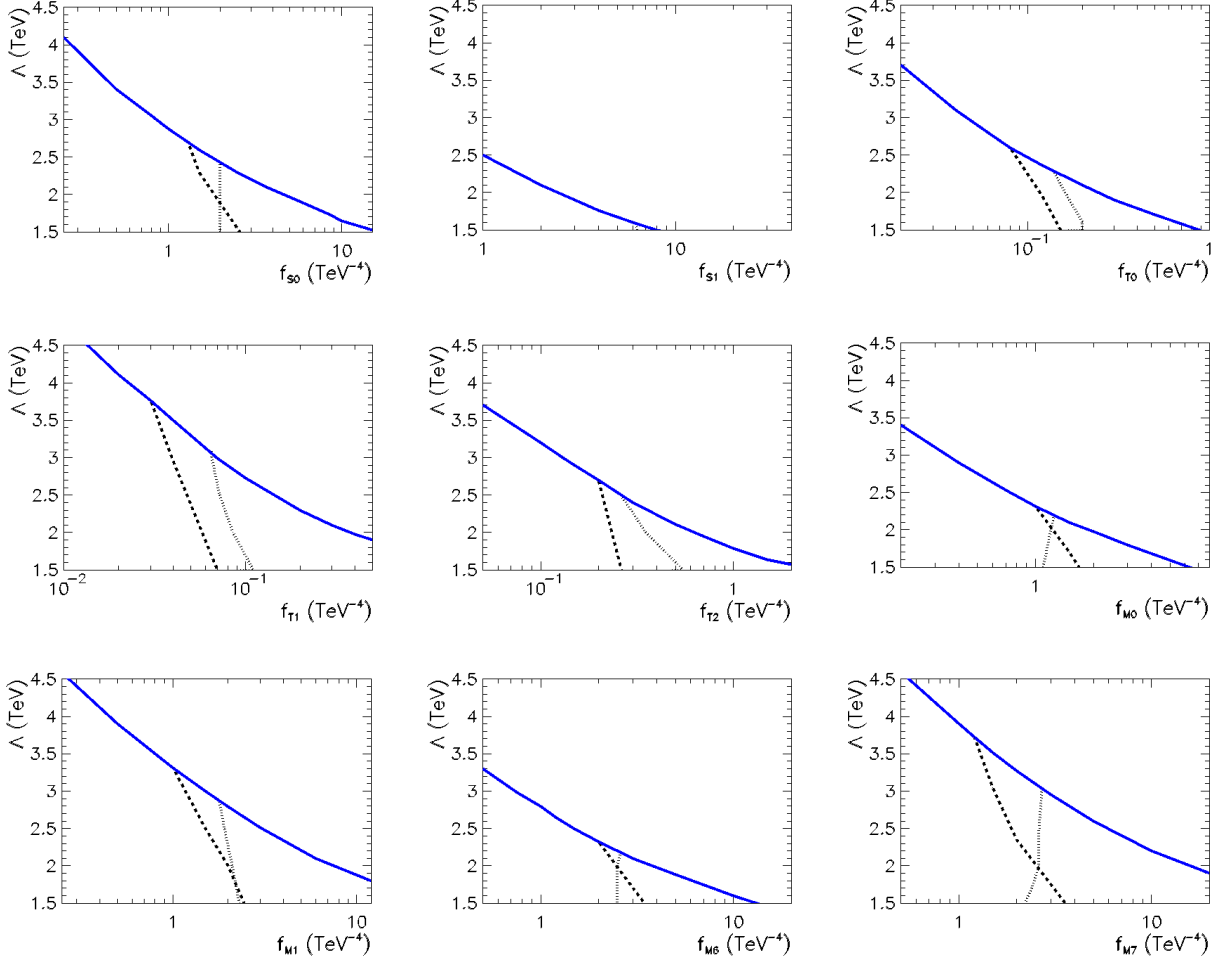

Figure 4: Regions in the Λ vs f (positive f values) space for dimension-8 operators in which a 5σ BSM signal can be observed and the EFT is applicable. The unitarity limit is shown in blue. Also shown are the lower limits for a 5σ signal significance from Eq. (1.9) (dashed lines) and the upper limit on 2σ EFT consistency (dotted lines). Assumed is $\sqrt{s} = 14$ TeV and an integrated luminosity of 3 ab^{-1}.

4 Conclusions and outlook

In this paper we have analyzed the prospects for discovering physics beyond the SM at the HL-LHC in the EFT framework applied to the VBS amplitudes, in the process $pp \rightarrow W^+W^+jj$. We have
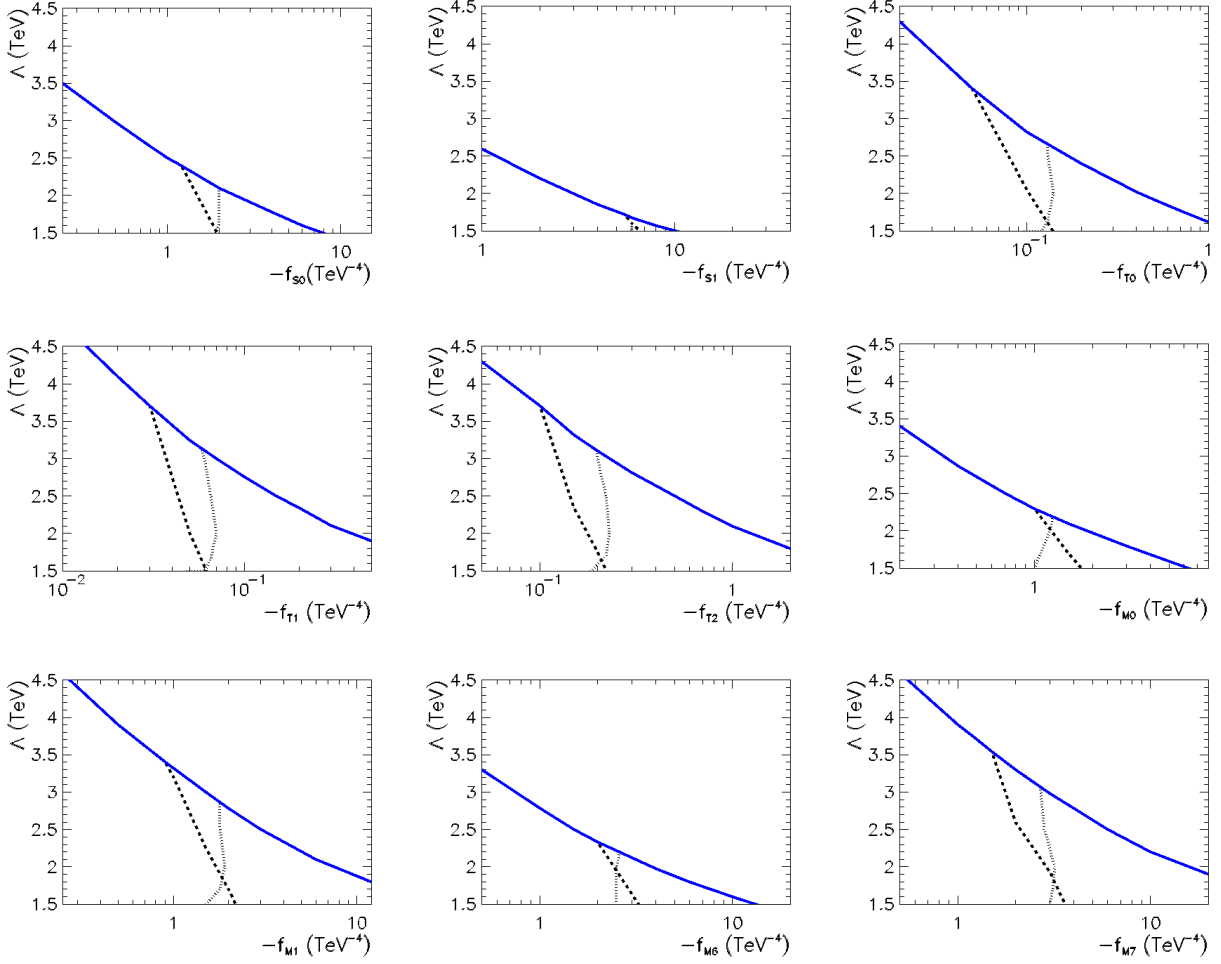
Figure 5: Regions in the Λ vs f (negative f values) space for dimension-8 operators in which a 5σ BSM signal can be observed and the EFT is applicable. For the meaning of curves see caption of Fig. 4. Assumed is $\sqrt{s} = 14$ TeV and an integrated luminosity of 3 ab^{-1}.
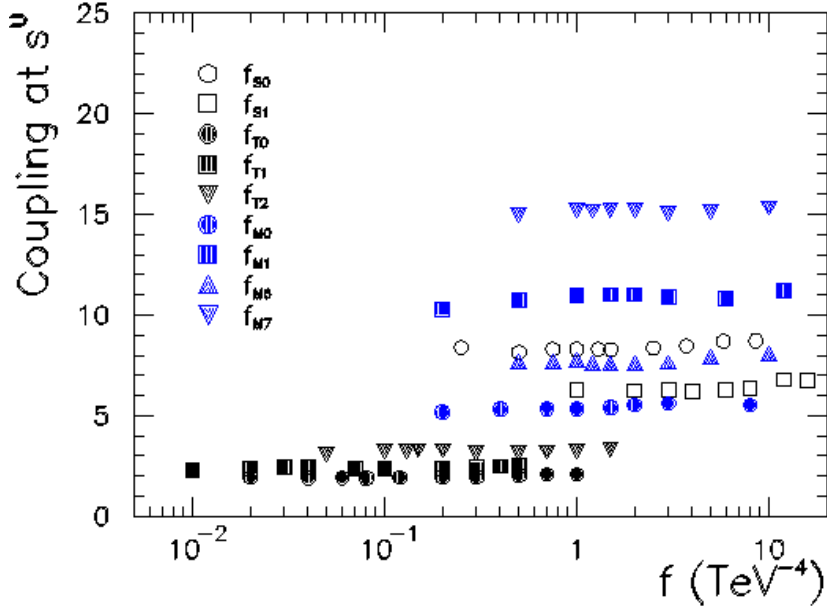
Figure 6: Maximum value $\sqrt{C_{max}}$ of the coupling constants related to individual dimension-8 operators, calculated at the energy where the unitarity limit is reached, as a function of the relevant f value.

introduced the concept of EFT "models" defined by the choice of higher dimension operators and values of the Wilson coefficients and analyzed "models" based on single dimension-8 operators at a time. We emphasize the role of the invariant mass M_{WW} whose distribution directly relates to the intrinsic range of validity of the EFT approach, $M_{WW} < \Lambda \leq M^U$, and the importance to tackle this issue correctly in data analysis in order to study the underlying BSM physics. While this is relatively simple (in principle) for final states where M_{WW} can be determined on an event-by-event basis, the value of M_{WW} is unfortunately not available in leptonic W decays. We argue that usage of EFT "models" in the analysis of purely leptonic W decay channels requires bounding the possible contribution from the region $M_{WW} > \Lambda$, no longer described by the "model", and ensuring it does not significantly distort the measured distributions compared to what they would have looked from the region of EFT validity alone.

We propose a data analysis strategy to satisfy the above requirements and verify in what ranges of the relevant Wilson coefficients such strategy can be successfully applied in a future analysis of the HL-LHC data. We find that, with a possible exception of $\mathcal{O}_{S1}$, all dimension-8 operators which affect the $WWWW$ quartic coupling have regions where a 5σ BSM signal can be observed at HL-LHC with 3 ab^{-1} of data, while data could be satisfactorily described using the EFT approach.

From such analysis it may be possible to learn something about the underlying UV completion of the full theory. Successful determination of a given f value, using a procedure that respects the EFT restricted range of applicability, will put non-trivial bounds on the value of Λ and consequently, the BSM coupling C. These bounds are rather weak for $\mathcal{O}_{T0}$, $\mathcal{O}_{T1}$ and $\mathcal{O}_{T2}$ operators, but potentially stronger for $\mathcal{O}_{M0}$, $\mathcal{O}_{M1}$, $\mathcal{O}_{M6}$ and $\mathcal{O}_{M7}$. In particular, applicability of the EFT in terms of these operators already requires $\Lambda \geq 2$ TeV, while stringent upper limits arise from the unitarity condition. Because of relatively low sensitivity to f_{S0} and f_{S1}, it will unfortunately be hard to learn much about

14

$W_L W_L$ physics using the EFT approach with dimension-8 operators.

It must be stressed that in this analysis we have only considered single dimension-8 operators at a time. Allowing non-zero values of more than one f at a time provides much more felixibility as far as the value of Λ is concerned, especially for those operators whose individual unitarity limits are driven by helicity combinations which contribute little to the total cross section. Consequently, regions of BSM observability and EFT consistency can only be larger than what we found here. Study of VBS processes in the EFT language can be the right way to look for new physics and should gain special attention in case the LHC fails to observe new physics states directly.

Consideration of other VBS processes and W decay channels may significantly improve the situation. In particular, the semileptonic decays, where one W^+ decays leptonically and the other W^+ into hadrons, have never been studied in VBS analyses because of their more complicated jet combinatorics and consequently much higher background. Progress in the implementation of W-jet tagging techniques based on jet substructure algorithms may render these channels interesting again. However, they are presently faced with two other experimental challenges. One is the precision of the M_{WW} determination which relies on the missing-E_T measurement resolution. The other one is poor control over the sign over the hadronic W. The advantages would be substantial. If M_{WW} can be reconstructed with reasonable accuracy, it is straightforward to fit f and Λ to the measured distribution in an EFT-consistent way even for arbitrarily large f. Existence of a high-M_{WW} tail above Λ is then not a problem, but a bonus, as it may give us additional hints about the BSM physics. Finally, because of the invariant mass issue, the ZZ scattering channel, despite its lowest cross section, may ultimately prove to be the process from which we can learn the most about BSM in case the LHC fails to discover new physics directly.

Acknowledgments

A   Unitarity bounds

The purpose of this section is to give an overview of the behavior of individual helicity amplitudes as a function of energy and their contributions to the total unpolarized cross section, with special attention paid to the partial wave unitarity constraints, in the SM and in its extensions to the EFT "models" discussed in this paper. We shall illustrate the main points using the operators $\mathcal{O}_{S0}$ and $\mathcal{O}_{T1}$. The choice is determined by the requirement that the s^U bounds for $W^+ W^+$ which we present below are stronger than for $W^+ W^-$ (often used in our analyses). The qualitative picture remains the same for the other operators as well. Analytical computations have been partially performed using a Mathematica code. All cross sections are computed with a $10°$ cut in the forward and backward scattering regions. Similarly, a $1°$ cut is applied for partial amplitudes, hence for s^U determination.

We begin by choosing a set of independent helicity amplitudes for $W^+ W^+$ scattering. Altogether,

there are 81 helicity amplitudes for this process but P and T discrete symmetries and the fact that the state has a symmetric wave function (Bose statistics) impose many relations between them and leave only 13 amplitudes as an independent set. We choose them as follows:

$$
\begin{array}{ccccccc}
---- & ---0 & ---+ & --00 & --0+ & --++ & -0-0 \\
-0-+ & -000 & -00+ & -+-+ & -+00 & 0000 &
\end{array}
\tag{A.1}
$$

Here $+$, $-$ and 0 denote the right-handed, left-handed and longitudinal polarizations, respectively; the first two symbols define the initial state and the last two symbols define the final state. These amplitudes contribute to the total cross section with multiplicities

$$
\begin{array}{ccccccc}
2 & 8 & 8 & 4 & 8 & 2 & 8 \\
16 & 8 & 8 & 4 & 4 & 1 &
\end{array}
$$

respectively, due to symmetry relations between all the 81 amplitudes. In the SM their energy dependence is at most flat but their magnitude can differ by orders of magnitude (see Table 2 for their energy dependence and the contribution of the corresponding polarized cross sections to the total unpolarized cross section at 1 TeV). The unpolarized cross section (decreasing like $1/s$) is saturated by just four of them, taking into account the corresponding multiplicities (see Fig. 7).

The next thing of interest for us is the scattering energy $\sqrt{s^U}$ at which partial wave unitarity is violated by different helicity amplitudes for the two operators considered in this section, according to the tree level criterion $|\text{Re}\{a_{J=0}\}| < 1/2$. This is shown in Table 3 for the $\mathcal{O}_{S0}$ operator (positive f) and in Table 4 for $\mathcal{O}_{T1}$ (negative f), as a function of the values of f. We see that partial wave unitarity is first violated in the 0000 amplitude for the first operator and in $----$ for the second one. Unitarity is violated at vastly different energies for different helicity amplitudes, depending on the operator considered. Some of them remain constant with energy, in particular some of those that saturate the SM total cross section. The leading energy dependences of the amplitudes and the contributions of polarized cross sections to the total unpolarized cross section at the lowest s^U where the first helicity amplitude violates partial wave unitarity are shown in Tables 5 and 6, respectively. One sees that for $\mathcal{O}_{S0}$, the 0000 cross section (related to the amplitude which violates unitarity first) gives about 35% of the total cross sections, independently of the value of f, for the corresponding values of minimal s^U. For $\mathcal{O}_{T1}$, it is the $----$ cross section, with an about 45% contribution to the total unpolorized cross section, independently of the value of f, for the corresponding values of minimal s^U. The rest of the unpolarized cross sections at the minimal s^U come (for both operators) from the helicity amplitudes that saturate the cross section in the SM, which either remain constant with energy (although weakly dependent on the value of f) or violate perturbative partial unitarity at a higher energy.

Unitarity bounds calculated from T-matrix diagonalization are virtually identical to those for the amplitude that determines the minimal s^U for $\mathcal{O}_{S0}$, while for $\mathcal{O}_{T1}$ they are about 10% lower.

Some examples of the energy dependence of the cross sections for both operators are shown in the following figures: for the total unpolarized cross sections with $\mathcal{O}_{S0}$ in Fig. 8, for polarized cross sections with $\mathcal{O}_{S0}$ in Fig. 10, for unpolarized with $\mathcal{O}_{T1}$ in Fig. 9, and for polarized with $\mathcal{O}_{T1}$ in Fig. 11. We observe that both operators show several similar interesting features. Below the partial wave unitarity minimal bounds s^U, sizable deviations from the SM predictions occur only for small energy intervals close to those bounds. They are mainly due to the interference term in Eq. (1.3) (see Figs. 8 and 9). The interference terms remain important also for a sizable range of energy above

16

the unitarity bounds, but eventually the $(BSM)^2$ term in Eq. (1.3) begins to dominate the energy dependence of the cross sections. The energy dependence of the unpolarized cross sections around the values of the minimal s^U is moreover somewhat weakened by the contribution from the helicity amplitudes that have not reached the unitarity limit.

helicity	iM(s,θ,f)	σ_ijkl
----	$-\dfrac{32\,i\,c_W^2\,\csc^2(\theta)\,M_Z^2}{v^2}$	100.
---0	$-\dfrac{2\,i\,\sqrt{2}\,c_W^3\cot(\theta)\,\csc^2(\theta)\,M_Z^3\left(\cos(2\theta)\left((4c_W^2+1)M_Z^2-M_h^2\right)+(28c_W^2-25)M_Z^2-7M_h^2\right)}{s^{3/2}\,v^2}$	2.6×10^{-3}
---+	$\dfrac{16\,i\,c_W^4\,M_Z^4}{s\,v^2}$	6.1×10^{-4}
--00	$\dfrac{2\,i\,c_W^2\,\csc^2(\theta)\,M_Z^2\left(\cos(2\theta)\left(M_Z^2-M_h^2\right)-3M_h^2-5M_Z^2\right)}{s\,v^2}$	4.8×10^{-3}
--0+	$\dfrac{4\,i\,\sqrt{2}\,c_W^3\cot(\theta)\,M_Z^3\left((4c_W^2+1)M_Z^2-M_h^2\right)}{s^{3/2}\,v^2}$	5.1×10^{-6}
--++	$\dfrac{8\,i\,c_W^4\,M_Z^4\left((4c_W^2+1)M_Z^2-M_h^2-4\csc^2(\theta)M_Z^2\right)}{s^2\,v^2}$	2.2×10^{-7}
-0-0	$\dfrac{8\,i\,c_W^2\,M_Z^2}{v^2\left(\cos(\theta)-1\right)}$	110.
-0-+	$-\dfrac{8\,i\,\sqrt{2}\,c_W^3\cot\left(\frac{\theta}{2}\right)M_Z^3}{\sqrt{s}\,v^2}$	0.42
-000	$\dfrac{2\,i\,\sqrt{2}\,c_W\cot(\theta)\,M_Z\,(M_Z-M_h)\,(M_h+M_Z)}{\sqrt{s}\,v^2}$	1.7×10^{-3}
-00+	$\dfrac{4\,i\,c_W^2\,M_Z^2\left(\cos(\theta)\left((4c_W^2+1)M_Z^2-M_h^2\right)-4c_W^2M_Z^2\right)}{s\,v^2\left(\cos(\theta)-1\right)}$	1.4×10^{-3}
-+-+	$-\dfrac{8\,i\,c_W^2\cot^2\left(\frac{\theta}{2}\right)M_Z^2}{v^2}$	170.
-+00	$-\dfrac{4\,i\,c_W^2\,M_Z^2\left((8c_W^2+1)M_Z^2+2\csc^2(\theta)\left(M_h^2-M_Z^2\right)-M_h^2\right)}{s\,v^2}$	2.4×10^{-3}
0000	$-\dfrac{2\,i\left(M_h^2+4\csc^2(\theta)M_Z^2-M_Z^2\right)}{v^2}$	7.8

Table 2: The leading energy behavior in the limit $s >> (\text{EW scale})^2$ of the scattering amplitude iM for all the 13 independent helicities in the SM case. In the third column shown are numerical values (in pb) of the contributions from the helicities to the total unpolarized cross section at 1 TeV; c_W is the cosine of the Weinberg mixing angle, v is the SM Higgs vev, θ is the scattering angle.
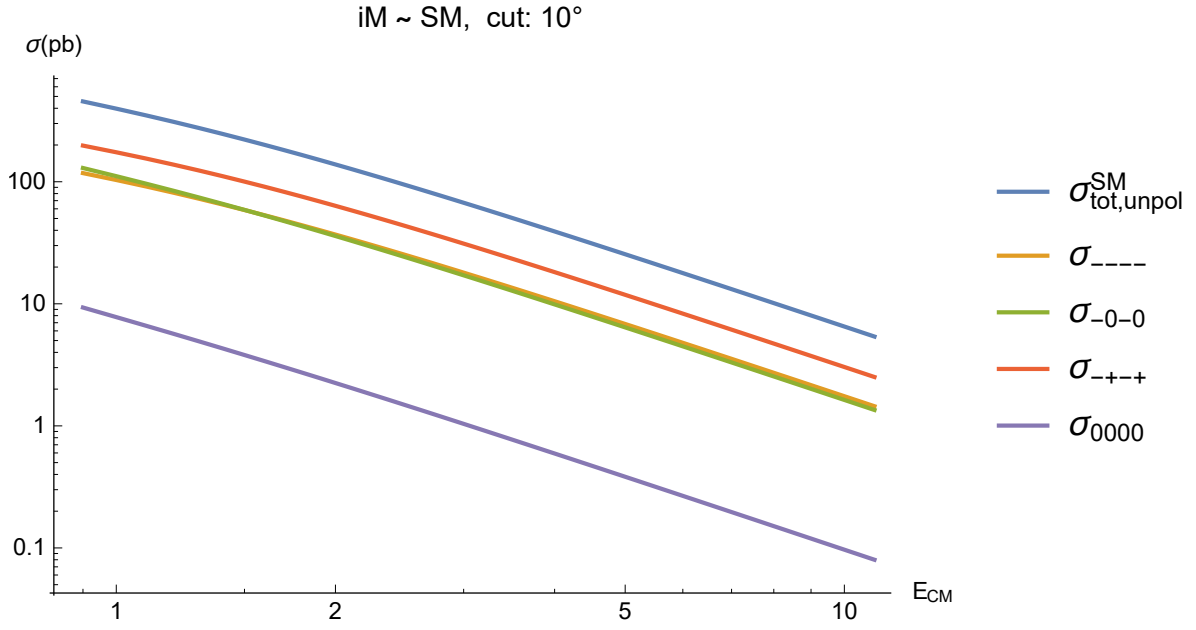
Figure 7: Illustration of the contributions of different helicities (multiplicity taken into account) to the total unpolarized cross section as a function of the center-of-mass collision energy ($E_{CM} \equiv \sqrt{s}$, in TeV) in the SM. The total cross section is shown in blue.

$$
\begin{pmatrix}
\text{helicity} & 0.01 & 0.1 & 1. & 10. \\
---- & \text{x} & \text{x} & \text{x} & \text{x} \\
---0 & \text{x} & \text{x} & \text{x} & \text{x} \\
---+ & \text{x} & \text{x} & \text{x} & \text{x} \\
--00 & 440. & 140. & 44. & 14. \\
--0+ & \text{x} & \text{x} & \text{x} & \text{x} \\
--++ & \text{x} & \text{x} & \text{x} & \text{x} \\
-0-0 & \text{x} & \text{x} & \text{x} & \text{x} \\
-0-+ & \text{x} & \text{x} & \text{x} & \text{x} \\
-000 & \text{x} & \text{x} & \text{x} & \text{x} \\
-00+ & \text{x} & \text{x} & \text{x} & \text{x} \\
-+-+ & \text{x} & \text{x} & \text{x} & \text{x} \\
-+00 & \text{x} & \text{x} & \text{x} & \text{x} \\
0000 & 7.5 & 4.2 & 2.4 & 1.3
\end{pmatrix}
$$

Table 3: Values of $\sqrt{s^U}$ (in TeV) for all the helicity amplitudes from the partial wave unitarity criterion for a chosen set of f_{S0} values (first row, in TeV^{-4}); "x" denotes no unitarity violation.

$$
\begin{pmatrix}
\text{helicity} & -0.01 & -0.1 & -1. & -10. \\
\texttt{----} & 5.3 & 3.0 & 1.7 & 0.96 \\
\texttt{---0} & 7.5\times10^7 & 7.5\times10^6 & 7.5\times10^5 & 7.5\times10^4 \\
\texttt{---+} & 1.7\times10^3 & 530. & 170. & 53. \\
\texttt{--00} & 440. & 140. & 44. & 14. \\
\texttt{--0+} & 74. & 34. & 16. & 7.4 \\
\texttt{--++} & 5.5 & 3.1 & 1.7 & 0.99 \\
\texttt{-0-0} & 2.5\times10^3 & 800. & 250. & 80. \\
\texttt{-0-+} & 69. & 32. & 15. & 6.9 \\
\texttt{-000} & 3.7\times10^7 & 3.7\times10^6 & 3.7\times10^5 & 3.7\times10^4 \\
\texttt{-00+} & 2.3\times10^3 & 740. & 230. & 74. \\
\texttt{-+-+} & 10. & 5.6 & 3.2 & 1.8 \\
\texttt{-+00} & 1.7\times10^3 & 530. & 170. & 53. \\
\texttt{0000} & \text{x} & \text{x} & \text{x} & \text{x}
\end{pmatrix}
$$

Table 4: Values of $\sqrt{s^U}$ (in TeV) for all the helicity amplitudes from the partial wave unitarity criterion for a chosen set of f_{T1} values (first row, in TeV^{-4}); "x" denotes no unitarity violation.

helicity	iM(s,Θ,f)	0.01	0.1	1.	10.
----	$4\,\mathbb{i}\,c_W^4\,f_{S0}\,M_Z^4 - \dfrac{32\,\mathbb{i}\,\csc^2(\Theta)\,c_W^2\,M_Z^2}{v^2}$	3.1	9.5	28.	70.
---0	$-\dfrac{2\,\mathbb{i}\,\sqrt{2}\,\cot(\Theta)\,\csc^2(\Theta)\,c_W^3\,M_Z^3\,\left(-7\,M_h^2+\left(28\,c_W^2-25\right)M_Z^2+\cos(2\Theta)\left(\left(4\,c_W^2+1\right)M_Z^2-M_h^2\right)\right)}{s^{3/2}\,v^2}$	1.1×10^{-9}	1.0×10^{-7}	7.9×10^{-6}	4.3×10^{-4}
---+	$\dfrac{16\,\mathbb{i}\,c_W^4\,M_Z^4}{s\,v^2}$	3.5×10^{-9}	1.1×10^{-7}	3.5×10^{-6}	1.1×10^{-4}
--00	$2\,\mathbb{i}\,s\,c_W^2\,f_{S0}\,M_Z^2$	1.3×10^{-6}	4.1×10^{-5}	1.3×10^{-3}	0.040
--0+	$\dfrac{4\,\mathbb{i}\,\sqrt{2}\,\cot(\Theta)\,c_W^3\,M_Z^3\,\left(\left(4\,c_W^2+1\right)M_Z^2-M_h^2\right)}{s^{3/2}\,v^2}$	6.0×10^{-13}	6.1×10^{-11}	6.0×10^{-9}	5.6×10^{-7}
--++	$4\,\mathbb{i}\,c_W^4\,f_{S0}\,M_Z^4$	3.7×10^{-14}	1.2×10^{-11}	3.7×10^{-9}	1.2×10^{-6}
-0-0	$\dfrac{8\,\mathbb{i}\,c_W^2\,M_Z^2}{v^2\,(\cos(\Theta)-1)}$	2.9	8.9	27.	71.
-0-+	$-\dfrac{8\,\mathbb{i}\,\sqrt{2}\,\cot\left(\frac{\Theta}{2}\right)c_W^3\,M_Z^3}{\sqrt{s}\,v^2}$	1.6×10^{-4}	1.6×10^{-3}	0.015	0.14
-000	$\dfrac{2\,\mathbb{i}\,\sqrt{2}\,\cot(\Theta)\,c_W\,M_Z\,(M_Z-M_h)\,(M_h+M_Z)}{\sqrt{s}\,v^2}$	1.7×10^{-6}	1.4×10^{-5}	9.4×10^{-5}	4.6×10^{-4}
-00+	$\dfrac{4\,\mathbb{i}\,c_W^2\,M_Z^2\,\left(\cos(\Theta)\left(\left(4\,c_W^2+1\right)M_Z^2-M_h^2\right)-4\,c_W^2\,M_Z^2\right)}{s\,v^2\,(\cos(\Theta)-1)}$	1.9×10^{-8}	5.5×10^{-7}	1.4×10^{-5}	3.1×10^{-4}
-+-+	$-\dfrac{8\,\mathbb{i}\,\cot^2\left(\frac{\Theta}{2}\right)c_W^2\,M_Z^2}{v^2}$	5.4	16.	48.	120.
-+00	$-\dfrac{4\,\mathbb{i}\,c_W^2\,M_Z^2\,\left(2\left(M_h^2-M_Z^2\right)\csc^2(\Theta)-M_h^2+\left(8\,c_W^2+1\right)M_Z^2\right)}{s\,v^2}$	2.3×10^{-8}	6.9×10^{-7}	1.9×10^{-5}	4.9×10^{-4}
0000	$\mathbb{i}\,s^2\,f_{S0}$	6.3	20.	62.	190.

Table 5: The leading energy dependence of the amplitudes (conventions as in Fig. 2) and the contribution of the polarized cross sections (in pb) to the total unpolarized cross sections at the minimal s^U for a chosen set of f_{S0} values (first row, in TeV^{-4}).

helicity	$i\mathcal{M}(s,\Theta,f)$	-0.01	-0.1	$-1.$	$-10.$
$----$	$2\,i\,s^2\,f_{T1}$	$24.$	$75.$	$230.$	$650.$
$---0$	$-i\,\sqrt{2}\,\sqrt{s}\,\cos(\Theta)\sin(\Theta)\,c_W^3\,f_{T1}\,M_Z^3$	1.3×10^{-8}	1.1×10^{-6}	7.1×10^{-5}	3.2×10^{-3}
$---+$	$-i\,s\,\sin^2(\Theta)\,c_W^2\,f_{T1}\,M_Z^2$	5.4×10^{-7}	1.7×10^{-5}	5.4×10^{-4}	0.017
$--00$	$-\frac{1}{2}\,i\,s\left(\cos(2\,\Theta)-9\right)c_W^2\,f_{T1}\,M_Z^2$	6.8×10^{-6}	2.1×10^{-4}	6.5×10^{-3}	0.19
$--0+$	$-\dfrac{i\,s^{3/2}\cos(\Theta)\sin(\Theta)\,c_W\,f_{T1}\,M_Z}{\sqrt{2}}$	2.1×10^{-4}	2.1×10^{-3}	0.021	0.21
$--++$	$\frac{1}{4}\,i\,s^2\left(\cos(2\,\Theta)+11\right)f_{T1}$	$18.$	$55.$	$170.$	$530.$
$-0-0$	$-\frac{1}{2}\,i\,s\,\sin^2(\Theta)\,c_W^2\,f_{T1}\,M_Z^2$	5.3	$16.$	$45.$	$110.$
$-0-+$	$i\,\sqrt{2}\,s^{3/2}\cos^3\!\left(\frac{\Theta}{2}\right)\sin\!\left(\frac{\Theta}{2}\right)c_W\,f_{T1}\,M_Z$	2.4×10^{-3}	0.024	0.24	2.3
-000	$-i\,\sqrt{2}\,\sqrt{s}\,\sin(2\,\Theta)\,c_W^3\,f_{T1}\,M_Z^3$	5.3×10^{-6}	3.9×10^{-5}	1.8×10^{-4}	1.5×10^{-3}
$-00+$	$\frac{1}{4}\,i\,s\left(4\cos(\Theta)+3\cos(2\,\Theta)+1\right)c_W^2\,f_{T1}\,M_Z^2$	3.6×10^{-7}	1.1×10^{-5}	3.7×10^{-4}	0.013
$-+-+$	$i\,s^2\cos^4\!\left(\frac{\Theta}{2}\right)f_{T1}$	$17.$	$52.$	$150.$	$380.$
$-+00$	$i\,s\,\sin^2(\Theta)\,c_W^2\,f_{T1}\,M_Z^2$	5.3×10^{-7}	1.6×10^{-5}	4.9×10^{-4}	0.015
0000	$\dfrac{2\,i\left(6\,v^2\,c_W^4\,f_{T1}\,M_Z^4+2\,v^2\cos(2\,\Theta)\,c_W^4\,f_{T1}\,M_Z^4-4\csc^2(\Theta)\,M_Z^2+M_Z^2-M_h^2\right)}{v^2}$	0.31	0.97	2.9	8.0

Table 6: The leading energy dependence of the amplitudes (conventions as in Fig. 2) and the contribution of the polarized cross sections (in pb) to the total unpolarized cross sections at the minimal s^U for a chosen set of f_{T1} values (first row, in TeV^{-4}).
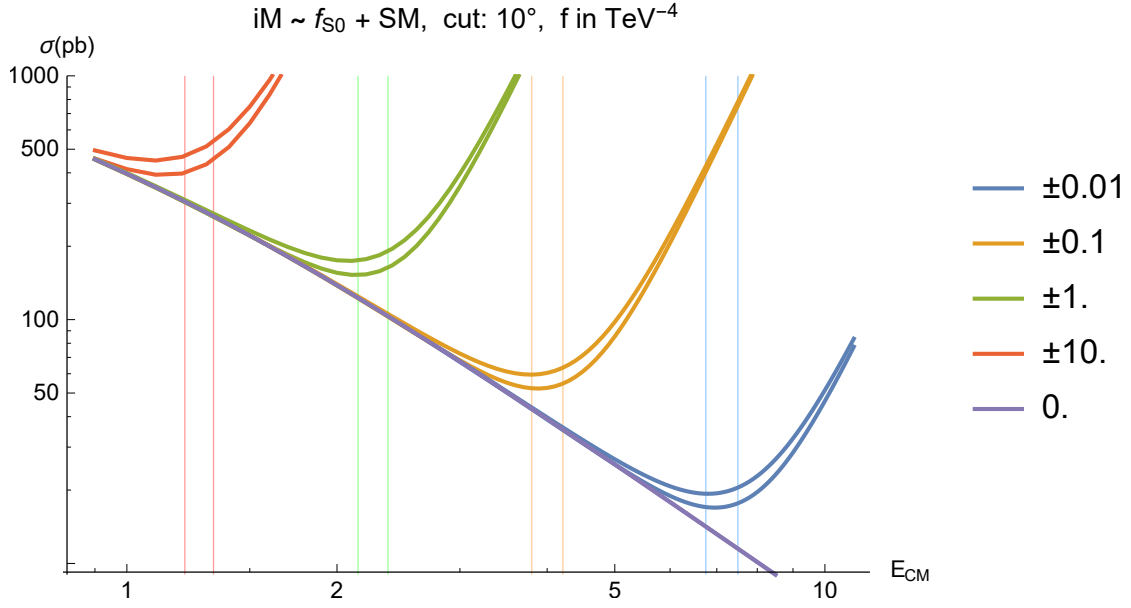
Figure 8: Energy dependence of the total unpolarized W^+W^+ cross sections ($E_{CM} \equiv \sqrt{s}$, in TeV) for a chosen set of f_{S0} values. Vertical lines denote the lowest $\sqrt{s^U}$ for each value of f (color correspondence). There is no color distinction between the signs, upper lines (and hence stronger $\sqrt{s^U}$ limits) correspond to negative values of f.
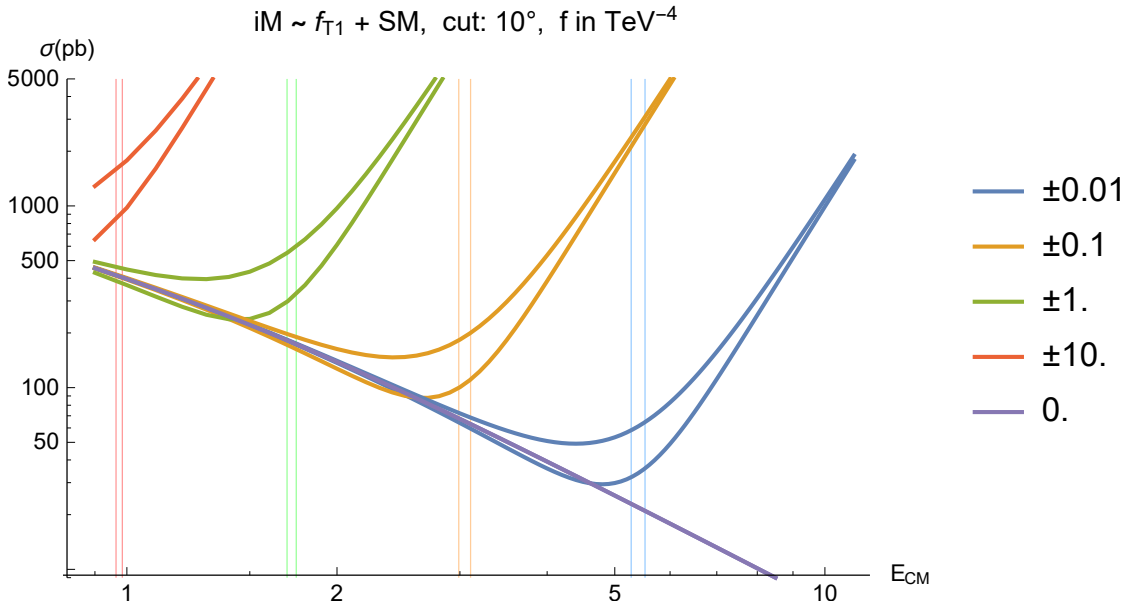

Figure 9: Energy dependence of the total unpolarized W^+W^+ cross sections ($E_{CM} \equiv \sqrt{s}$, in TeV) for a chosen set of f_{T1} values. Vertical lines denote the lowest $\sqrt{s^U}$ for each value of f (color correspondence). There is no color distinction between the signs, upper lines (and hence stronger $\sqrt{s^U}$ limits) correspond to negative values of f.
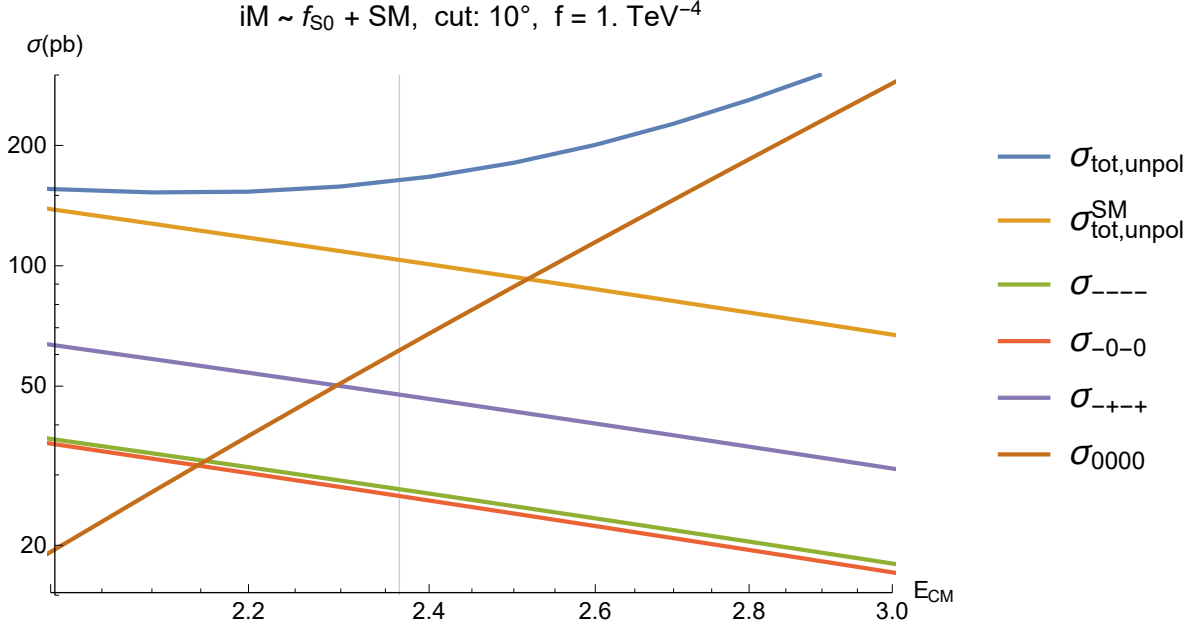
21

Figure 10: Contributions of the polarized cross sections (multiplicity taken into account) to the total unpolarized cross section as a function of the center-of-mass collision energy ($E_{CM} \equiv \sqrt{s}$, in TeV) for $f_{S0} = 1.$ TeV^{-4}. The total cross section is shown in blue, the total cross section in the SM is shown in orange. The remaining polarized cross sections are negligibly small.
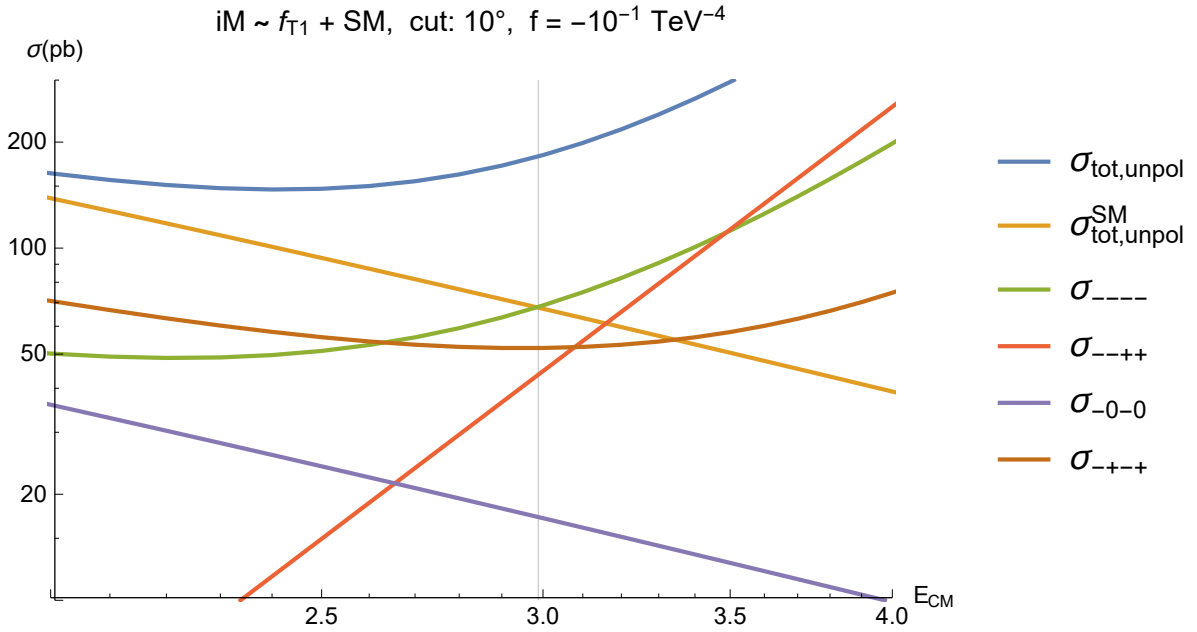

Figure 11: Contributions of the polarized cross sections (multiplicity taken into account) to the total unpolarized cross section as a function of the center-of-mass collision energy ($E_{CM} \equiv \sqrt{s}$, in TeV) for $f_{T1} = -0.1$ TeV^{-4}. The total cross section in shown in blue, the total cross section in the SM is shown in orange. The remaining polarized cross sections are negligibly small.

References

[1] G. F. Giudice, C. Grojean, A. Pomarol and R. Rattazzi, JHEP **0706** (2007) 045, doi:10.1088/1126-6708/2007/06/045 [hep-ph/0703164].

[2] A. Biektter, A. Knochel, M. Krämer, D. Liu and F. Riva, Phys. Rev. D **91** (2015) 055029, doi:10.1103/PhysRevD.91.055029 [arXiv:1406.7320 [hep-ph]].

[3] D. Liu, A. Pomarol, R. Rattazzi and F. Riva, JHEP **1611** (2016) 141, doi:10.1007/JHEP11(2016)141 [arXiv:1603.03064 [hep-ph]].

[4] R. Contino, A. Falkowski, F. Goertz, C. Grojean and F. Riva, JHEP **1607** (2016) 144, doi:10.1007/JHEP07(2016)144 [arXiv:1604.06444 [hep-ph]].

[5] A. Azatov, R. Contino, C. S. Machado and F. Riva, Phys. Rev. D **95** (2017) no.6, 065014, doi:10.1103/PhysRevD.95.065014 [arXiv:1607.05236 [hep-ph]].

[6] R. Franceschini, G. Panico, A. Pomarol, F. Riva and A. Wulzer, arXiv:1712.01310 [hep-ph].

[7] A. Falkowski, M. Gonzalez-Alonso, A. Greljo, D. Marzocca and M. Son, JHEP **1702** (2017) 115, doi:10.1007/JHEP02(2017)115 [arXiv:1609.06312 [hep-ph]].

[8] G. Aad *et al.* [ATLAS Collaboration], Phys. Rev. Lett. **113** (2014) no.14, 141803, doi:10.1103/PhysRevLett.113.141803 [arXiv:1405.6241 [hep-ex]].

[9] V. Khachatryan *et al.* [CMS Collaboration], Phys. Rev. Lett. **114** (2015) no.5, 051801, doi:10.1103/PhysRevLett.114.051801 [arXiv:1410.6315 [hep-ex]]. M. Aaboud *et al.* [ATLAS Collaboration], Phys. Rev. D **96** (2017) no.1, 012007, doi:10.1103/PhysRevD.96.012007 [arXiv:1611.02428 [hep-ex]].

[10] A. M. Sirunyan *et al.* [CMS Collaboration], arXiv:1709.05822 [hep-ex].

[11] C. Degrande *et al.*, arXiv:1309.7890 [hep-ph].

[12] O.J.P. Éboli and M.C. Gonzalez-Garcia, Phys. Rev. D **93** (2016) no.9, 093013, doi:10.1103/PhysRevD.93.093013 [arXiv:1604.03555 [hep-ph]].

[13] For a combined analysis of LEP and Run I LHC data, see e.g. A. Butter, O.J.P. Éboli, J. Gonzalez-Fraile, M.C. Gonzalez-Garcia, T. Plehn and M. Rauch, JHEP **1607** (2016) 152, doi:10.1007/JHEP07(2016)152 [arXiv:1604.03105 [hep-ph]].

[14] G. Aad *et al.* [ATLAS Collaboration], Phys. Rev. D **93** (2016) no.9, 092004, doi:10.1103/PhysRevD.93.092004 [arXiv:1603.02151 [hep-ex]].

[15] A. M. Sirunyan *et al.* [CMS Collaboration], Phys. Lett. B **774** (2017) 682, doi:10.1016/j.physletb.2017.10.020 [arXiv:1708.02812 [hep-ex]].

[16] J. Alwall *et al.*, JHEP **07** (2014) 079, doi:10.1007/JHEP07(2014)079 [arXiv:1405.0301 [hep-ph]].

[17] K. Arnold *et al.*, Comput. Phys. Commun. **180** (2009) 1661, doi:10.1016/j.cpc.2009.03.006 [arXiv:0811.4559 [hep-ph]]; J. Baglio *et al.* arXiv:1107.4038 [hep-ph], arXiv:1404.3940 [hep-ph].

[18] T. Sjostrand, S. Mrenna, P. Skands, JHEP **0605** (2016) 026, doi:10.1088/1126-6708/2006/05/026 [arXiv:hep-ph/0603175].

[19] K. Doroba *et al.*, Phys. Rev. D **86** (2012) no.3, 036011, doi:10.1103/PhysRevD.86.036011 [arXiv:1201.2768 [hep-ph]].

[20] S. Todt, Ph.D. Thesis CERN-THESIS-2015-018, TU Dresden, 2015.

[21] C. Degrande *et al.*, arXiv:1309.7452 [physics.comp-ph].